Int J Thermophys (2009) 30:1791–1810
DOI 10.1007/s10765-009-0684-1

Henry's Law Constant from Molecular Simulation: A Systematic Study of 95 Systems

Yow-Lin Huang · Svetlana Miroshnichenko · Hans Hasse · Jadran Vrabec

Received: 19 September 2009 / Accepted: 12 November 2009 / Published online: 23 November 2009

Abstract A set of molecular models from prior work for 78 pure substances is taken as a basis for systematically studying the temperature dependence of the Henry's law constant in pure solvents. All 95 binary mixtures that can be formed out of these 78 components, and for which experimental Henry's law constant data are available, are investigated by molecular simulation. The mixture models are based on the modified Lorentz–Berthelot combining rule that contains one binary interaction parameter which is adjusted to the Henry's law constant at one temperature or, in preceding work, to the binary system vapor pressure. The predictions from the molecular models of the 95 binary mixtures are compared to available experimental data. In most cases, the molecular models yield good predictions for the gas solubility. It is found that the models are generally capable of yielding reliable data both at infinite dilution and at finite mole fractions.

Keywords Henry's law constant · Vapor–liquid equilibria · Molecular mixture model · Unlike interaction

Electronic supplementary material The online version of this article (doi:10.1007/s10765-009-0684-1) contains supplementary material, which is available to authorized users.

Y.-L. Huang · S. Miroshnichenko · J. Vrabec (✉)
Lehrstuhl für Thermodynamik und Energietechnik, Universität Paderborn,
Warburger Straße 100, 33098 Paderborn, Germany
e-mail: jadran.vrabec@upb.de

H. Hasse
Lehrstuhl für Thermodynamik, Technische Universität Kaiserslautern,
Erwin-Schrödinger-Straße 44, 67663 Kaiserslautern, Germany

1 Introduction

Thermodynamic data on the distribution of the components in coexisting vapor and liquid phases are essential for a wide range of technical applications. A common classification distinguishes between mixtures in which the components have a similar volatility and mixtures in which the components have a strongly differing volatility. In the first case, for binary mixtures, considerable amounts of both components can be found in the coexisting phases, and the characterization of the equilibrium requires, for a given pair of temperature and pressure, both the liquid composition and the vapor composition. Depending on the mixture, a large variation in the distribution of the components is found, leading to qualitatively different forms of the two-phase envelope, such as for zeotropic or azeotropic systems. In the second case, the liquid overwhelmingly contains the component with low volatility (i.e., solvent), while the vapor is composed mainly of the volatile component (i.e., solute). The two-phase envelope is thus wide and has a characteristic shape. For example, it is observed at constant temperature that the solute mole fraction in the liquid increases approximately linearly with the pressure. This has given rise to a condensed characterization of the phase equilibrium in such cases through the Henry's law constant H_i. Considering a mixture of two components, classically the phase equilibrium condition for the solute i at a specified pair of temperature T and pressure p is then given by [1,2]

$$H_i \exp\left\{\frac{1}{k_B T}\int_{p_S^s}^{p} v_i^{\infty} \mathrm{d}p\right\} x_i \gamma_i^* = p\, y_i\, \phi_i, \tag{1}$$

where x_i and y_i are the solute mole fractions in the saturated liquid and vapor phases, respectively, v_i^{∞} is the partial molar volume of the solute at infinite dilution in the liquid, and k_B is the Boltzmann constant. Non-idealities of the liquid phase are considered by the activity coefficient normalized according to Henry's law γ_i^*, and of the vapor phase by the fugacity coefficient ϕ_i. The exponential term, known as the Krichevski–Kasarnovski correction [3], accounts for the dependence of the chemical potential of the solute on the pressure p, where p_S^s stands for the pure solvent vapor pressure.

For the equilibrium condition of the solvent S, typically the extended form of Raoult's law is used [1,2]

$$p_S^s \phi_S^s \exp\left\{\frac{1}{k_B T}\int_{p_S^s}^{p} v_S \mathrm{d}p\right\} x_S \gamma_S = p\, y_S\, \phi_S, \tag{2}$$

where ϕ_S^s is the fugacity coefficient of the solvent at saturation, γ_S is the activity coefficient normalized according to Raoult's law, and v_S is the volume of the liquid solvent. Note that the exponential term is known as the Poynting correction.

Often the non-ideality of the phases and the Krichevski–Kasarnovski correction as well as the Poynting correction are neglected, so that a very simple expression for

the phase equilibrium remains, which only includes the pure substance solvent vapor pressure and the Henry's law constant.

The aim of this work is to predict the temperature dependence of the Henry's law constant in a systematic manner for a wide range of solutes and solvents by molecular modeling and simulation. The predictions are based on the polar two-center Lennard–Jones (2CLJ) potential that has been parameterized in previous work of our group for 78 components [4,5]. These are 78 small molecules consisting of up to nine atoms that belong to different classes of fluids, including noble gases, alkanes, halogens, and numerous refrigerants. For many of the 78 molecules, the polar 2CLJ model is only a crude assumption. For example, the asymmetry of molecules is neglected, and the polar interaction is always aligned along the molecular axis. Also the polarizability, which is often assumed to be a crucial molecular property for thermodynamics, is only implicitly considered by Lennard–Jones interaction sites. Furthermore, the internal degrees of freedom are neglected, as the polar 2CLJ models are rigid.

Following a combinatorial approach, all binary mixtures for which experimental data on the Henry's law constant are available were studied here. This work extends a preceding publication on binary vapor–liquid equilibria (VLE) [6], where the same group of components has been regarded in the same combinatorial sense but at different conditions, i.e., at finite mole fractions. Such data are termed as VLE data in the following. Due to the fact that for 29 binary combinations, both VLE [6] and Henry's law constant data are available, it was also investigated here whether molecular models are capable of yielding consistent results for both types of data.

Molecular modeling and simulation have been used for more than two decades for calculating the Henry's law constant. In the early works [7–10], usually model mixtures of Lennard–Jones spheres without reference to real fluids were considered. Lotfi and Fischer [11] also simulated mixtures of Lennard–Jones spheres, however, they applied them to real fluid systems such as He in liquid CH_4 or Ne in liquid Kr. The influence of the unlike interaction between the two molecule species was also investigated by applying different combining rules [11].

Mixtures of real components became better accessible through the development of simulation methodology and computing infrastructure. For example, Boulougouris et al. [12] calculated the solubility of CH_4 in liquid C_2H_6 and of the same solute in liquid water. Due to their technical importance, the solubility of larger hydrocarbons such as *n*-butane, *n*-hexane, cyclohexane, or benzene in liquid water was also studied [13,14]. Other systems, including CO_2 in liquid water [15] or O_2 in liquid benzene [16], were investigated as well.

The Industrial Fluid Property Simulation Collective [17] challenged the molecular simulation community in 2004 to predict the Henry's law constant for Ar, N_2, CH_4, and C_2H_6 in liquid ethanol. The submitted contributions have shown the capability of the molecular approach to determine this thermodynamic property [18–22].

In terms of simulation methodology, there is a variety of possibilities for determining the Henry's law constant. The most straightforward route is to sample the phase space of the solvent either by molecular dynamics or Monte-Carlo and to calculate the chemical potential of the solute at infinite dilution through insertions of test molecules by Widom's method [23]. However, if the density of the solvent is very high, e.g., in

the case of liquid water around ambient conditions, successful test molecule insertions become highly unlikely, which deteriorates the statistics. Solutions to this problem are discussed in a recent review [1].

2 Experimental Database

In this work, experimental data were predominately retrieved using the Dortmunder Datenbank (DDB) [24]. Theoretically, out of the $N = 78$ components modeled in [4,5], $N(N-1)/2 = 3003$ binary mixtures can be formed, but of course, by far not all of these systems have been studied experimentally. For 95 systems, experimental Henry's law constant data were found in 72 publications [25–96]; thereof, for 29 binary mixtures experimental VLE data are also available [6].

The 95 binary systems studied here include 41 of the 78 pure components; cf. Table 1 for the full component list including their CAS RN numbers for proper identification. Please note that the ASHRAE nomenclature is used in the following due to its brevity, despite its deficiencies [97]. Of the 41 components, 20 act as solutes, 15 as solvents, and six as solutes and solvents, since they are studied in mixtures with less and more volatile components, cf. Table 1.

The 95 binary systems studied are listed in Table 2, together with a reference to the experimental H_i data, indicating the subgroup of 29 systems for which experimental VLE data are available as well.

3 Pure Fluid Models

In this work, 41 polar 2CLJ-based molecular models were used, taken from [4,5]. These are five spherical non-polar (1CLJ) models for noble gases and CH_4, one spherical dipolar (1CLJD) model for R30, furthermore 16 elongated dipolar (2CLJD) models which include CO and numerous refrigerants, and finally 19 elongated quadrupolar (2CLJQ) models, which include N_2, O_2, alkanes, refrigerants, and CO_2.

A detailed description of the polar 2CLJ pair potential is provided in [6] and not repeated here. Generally, polar 2CLJ models have four parameters: size σ, energy ϵ, elongation L, and dipole moment μ or quadrupole moment Q; Stockmayer models have a vanishing elongation, while the non-polar spherical LJ models have only two parameters: σ and ϵ. Both their elongation and polarity are zero. Model parameters were adjusted in [4,5] to experimental pure fluid VLE data using global correlations of critical temperature, saturated liquid density, and vapor pressure as functions of these molecular parameters [98,99]. These pure substance model parameters are not repeated here. Typically, the deviations between the molecular models and the experiment are below 1 % for the saturated liquid density and below 3 % for the vapor pressure [4,5].

It should be noted that a wide range of polar moments are covered by the 41 pure substance models. Starting from a non-existent polar moment in the case of the noble gases and CH_4, it ranges up to 1.5984×10^{-29} C · m (4.7919 D) for the dipolar R130a and up to 5.3847×10^{-39} C · m^2 (16.143 DÅ) for the quadrupolar R1110.

Table 1 List of the 41 components studied in the present work, where *i* indicates solutes and S solvents

Fluid	CAS RN	Type	Fluid	CAS RN	Type
Non-polar, 1CLJ			*Quadrupolar, 2CLJQ*		
Ne	7440-37-1	*i*	N_2	7727-37-9	*i*
Ar	13965-95-2	*i*	O_2	7782-44-7	*i*
Kr	7439-90-9	*i*	Cl_2	7782-50-5	*i*/S
Xe	7440-63-3	*i*	CO_2	124-38-9	*i*/S
CH_4	74-82-8	*i*	CS_2	75-15-0	S
Dipolar, 1CLJD			C_2H_2	74-86-2	*i*
R30 (CH_2Cl_2)	75-09-2	S	C_2H_4	74-85-1	*i*
Dipolar, 2CLJD			C_2H_6	74-84-0	*i*
CO	630-08-0	*i*	Propylene ($CH_3-CH=CH_2$)	115-07-1	*i*/S
R11 ($CFCl_3$)	75-69-4	S	SF_6	2551-62-4	*i*/S
R12 (CF_2Cl_2)	75-71-8	*i*	R10 (CCl_4)	56-23-5	S
R13 (CF_3Cl)	75-72-9	*i*	R14 (CF_4)	75-73-0	*i*
R20 ($CHCl_3$)	67-66-3	S	R113 ($CFCl_2-CF_2Cl$)	76-13-1	S
R20B3 ($CHBr_3$)	75-25-2	S	R114 (CF_2Cl-CF_2Cl)	76-14-2	S
R22 (CHF_2Cl)	75-45-6	*i*	R116 (C_2F_6)	76-16-4	*i*
R23 (CHF_3)	75-46-7	*i*	R150B2 (CH_2Br-CH_2Br)	106-93-4	S
R40 (CH_3Cl)	74-87-3	*i*/S	R1110 (C_2Cl_4)	127-18-4	S
R130a ($CH_2Cl-CCl_3$)	630-20-6	S	R1114 (C_2F_4)	116-14-3	*i*
R140 ($CHCl_2-CH_2Cl$)	79-00-5	S	R1120 ($CHCl=CCl_2$)	79-01-6	S
R140a (CCl_3-CH_3)	71-55-6	S			
R150a ($CHCl_2-CH_3$)	75-34-3	S			
R161 (CH_2F-CH_3)	74-96-4	*i*			
R1132 ($CF_2=CH_2$)	75-38-7	*i*			
R1140 ($CHCl=CH_2$)	75-01-4	*i*/S			

The model parameters were taken from [4,5]

4 Henry's Law Constant from Molecular Models

Several approaches have been proposed in the literature to obtain the Henry's law constant on the basis of molecular models. Here, a straightforward route was followed. The Henry's law constant H_i is related to the residual chemical potential of the solute i at infinite dilution in the solvent ${\mu_i}^\infty$ [7,18] by

$$H_i = \rho_S k_B T \exp\left({\mu_i}^\infty/(k_B T)\right), \tag{3}$$

where ρ_S is the density of the solvent in its saturated liquid state.

In order to evaluate ${\mu_i}^\infty$, a molecular dynamics simulation applying Widom's test particle method [23] was used here. Therefore, test molecules representing the solute i were inserted into the pure saturated liquid solvent after each time step at random spatial coordinates, and the potential energy ψ_i between the solute test molecule i and all solvent molecules was calculated within the cut-off radius by

Table 2 Binary interaction parameter ξ_H adjusted to the Henry's law constant, experimental data used for the adjustment with reference, and simulation results with adjusted ξ_H

Mixture (i + S)	Category	ξ_H	T (K)	H_i^{sim} (MPa)	H_i^{exp} (MPa)	Ref.
$O_2 + Cl_2$	3	0.993	298	66.5(4)	66.3	[25]
$CO_2 + Cl_2$†	1	0.920	298.15	11.3(1)	11.2	[25]
$Xe + CO_2$	1	0.904	283.15	8.7(2)	8.7	[26]
$O_2 + CO_2$†	3	0.979	223.75	53.0(5)	53.0	[27]
$Ar + CS_2$	1	0.901	298.15	208.9(3)	209.2	[28,29]
$Kr + CS_2$	3	0.966	298.15	57.2(4)	57.7	[30]
$Xe + CS_2$	3	0.999	298	9.8(2)	9.7	[30]
$CH_4 + CS_2$	1	0.984	298.15	78(2)	80	[30,31]
$N_2 + CS_2$	1	0.905	298.15	463(6)	456	[30–32]
$O_2 + CS_2$	3	0.859	298.15	231(2)	230	[33]
$Cl_2 + CS_2$	1	0.991	298	0.93(3)	0.96	[34]
$CO + CS_2$	3	0.968	298	302(4)	303	[33]
$CO_2 + CS_2$†	1	0.877	306.36	34.1(5)	33.6	[31,35]
$C_2H_2 + CS_2$	1	0.942	288.15	17.5(6)	17.5	[36]
$C_2H_4 + CS_2$	3	0.995	298	15.7(5)	15.7	[37]
$C_2H_6 + CS_2$	3	0.992	298.15	9.8(4)	9.4	[28,30]
Propylene + CS_2	3	0.870	298.15	20(2)	19	[30]
$SF_6 + CS_2$	1	0.862	288.29	117(6)	110	[30,31]
R14 + CS_2	1	0.813	308	484(14)	476	[38]
N_2 + Propylene†	4	0.959	180	52.1(9)	–	[39]
$N_2 + SF_6$	3	1.400	300.15	8.34(3)	8.33	[40]
Ar + R10†	2	0.964	348.15	77.9(5)	74.1	[29,42]
Kr + R10	5	1.049	350	31.2(2)	–	[41,43]
CH_4 + R10	5	1.068	350	38.3(3)	–	[44]
N_2 + R10	5	0.899	340	134(1)	–	[45–47]
O_2 + R10	5	0.888	350	77.9(4)	–	[46–51]
Cl_2 + R10	1	0.972	344.15	2.0(2)	2.0	[52–56]
CO_2 + R10	4	0.808	340	18.2(1)	–	[35,48,57–60]
C_2H_2 + R10†	1	0.859	323.15	11.4(1)	11.4	[36]
C_2H_4 + R10†	1	0.978	333.15	11.0(4)	11.1	[37,61–63]
C_2H_6 + R10	5	1.043	350	8.3(1)	–	[62,64]
Propylene + R10†	1	1.005	333.15	2.8(9)	2.8	[62,63]
SF_6 + R10	4	0.834	361	26.6(7)	–	[38,41]
R12 + R10†	4	0.991	330	1.9(10)	–	[65]
R13 + R10	4	0.943	330	12.6(3)	–	[65]
R14 + R10	4	0.794	350	82(1)	–	[38]
R22 + R10†	5	0.929	350	4.07(7)	–	[66]
R23 + R10	5	0.725	380	32.3(3)	–	[67,68]
R40 + R10	4	0.925	350	2.23(2)	–	[69–72]
R161 + R10	4	0.959	350	2.34(4)	–	[73,74]

Table 2 continued

Mixture (i + S)	Category	ξ_H	T (K)	H_i^{sim} (MPa)	H_i^{exp} (MPa)	Ref.
R13 + R11†	1	0.975	273.15	2.56(7)	3.42	[75]
R22 + R11†	1	0.956	273.15	0.68(2)	0.92	[75]
R23 + R11†	1	0.802	303.15	14.0(1)	14.3	[67,76]
N_2 + R20	3	0.905	298.15	196.9(3)	196.1	[77]
O_2 + R20	3	0.833	289.65	140.8(2)	140.7	[78]
Cl_2 + R20	1	0.985	298.15	0.6(8)	0.7	[52]
C_2H_4 + R20†	4	1.001	390	15.2(2)	–	[63]
Propylene + R20†	4	0.975	390	6.79(7)	–	[63]
R22 + R20	3	0.950	293.15	2 (2)	1.7	[66]
R40 + R20	3	0.991	298.15	0.4(13)	0.5	[72]
R161 + R20	1	0.921	293.15	2 (2)	1.7	[73]
Kr + R20B3	3	0.956	295.15	61(1)	61	[43]
CH_4 + R30	1	0.893	303.15	80.8(8)	81.0	[79]
Cl_2 + R30	1	1.036	298.15	0.474(6)	0.483	[52]
CO_2 + R30†	1	0.868	310.93	10.38(7)	10.38	[80]
CH_4 + R40	3	1.011	293.15	32.8(3)	32.8	[81]
Ne + R113	2	0.928	298.15	116.9(1)	116.9	[82]
Ar + R113†	1	1.027	298.06	32.7(2)	32.7	[83]
Xe + R113	2	1.120	298.15	2.82(3)	2.7	[82]
CH_4 + R113†	1	1.044	308.15	20.8(1)	20.8	[83]
N_2 + R113	1	0.980	298.13	52.5(4)	52.5	[83]
CO_2 + R113	1	0.870	308.50	6.4(5)	6.49	[83]
C_2H_4 + R113	1	0.908	343.15	10.42(6)	10.50	[84]
C_2H_6 + R113	1	1.020	298.08	3.64(4)	3.76	[82,85,86]
SF_6 + R113†	1	0.894	319	6.6(1)	5.6	[38,83,87]
R14 + R113	1	0.858	278.40	18.5(5)	18.5	[38]
R116 + R113	2	0.998	300.73	3 (2)	3.6	[82,86]
R1114 + R113	1	0.946	298.15	3.3(9)	3.4	[88]
R1132 + R113	2	0.978	363.15	6.2(2)	6.2	[88]
N_2 + R114	2	1.196	313.15	18.6(1)	18.6	[89]
SF_6 + R114†	1	1.050	277	0.7(5)	1.02	[87]
R23 + R114†	3	0.732	303.15	9.45(7)	9.44	[67]
Cl_2 + R130a†	1	0.915	373	4.2(1)	4.2	[90]
Cl_2 + R140†	4	0.948	450	8.45(3)	–	[90]
C_2H_2 + R140	1	0.952	440	17.67(8)	–	[91]
R1140 + R140†	4	0.980	450	5.25(3)	–	[92]
Cl_2 + R140a†	1	0.930	281	0.7(4)	0.5	[90]
CO_2 + R140a†	3	0.889	294.26	6.57(6)	6.63	[59]
C_2H_2 + R140a	1	0.914	323.15	8.86(7)	7.52	[91]
R1140 + R140a	1	0.928	323.15	1.23(3)	1.24	[91]

Table 2 continued

Mixture (i + S)	Category	ξ_H	T (K)	H_i^{sim} (MPa)	H_i^{exp} (MPa)	Ref.
Cl_2 + R150a†	4	0.967	360	2.8(2)	–	[90]
C_2H_2 + R150a	4	0.965	360	9.18(6)	–	[93]
Cl_2 + R150B2	3	0.994	313.15	0.8(16)	0.9	[56]
CO + R150B2	3	0.909	298.15	369.1(6)	370.7	[94]
O_2 + R1110	5	0.926	380	87.6(2)	–	[50,51]
Propylene + R1110†	4	1.011	380	5.4(1)	–	[63]
R23 + R1110	5	0.664	380	60.0(7)	–	[67,68]
O_2 + R1120	5	0.961	340	88.3(2)	–	[51]
CO_2 + R1120	5	0.829	310	16.3(5)	–	[95]
C_2H_2 + R1120	5	0.847	314	13.1(6)	–	[95]
Propylene + R1120†	1	0.983	303.15	2.0(2)	1.9	[63,96]
C_2H_2 + R1140	1	1.008	242.15	1.3(11)	1.3	[93]

In cases where the experimental Henry's law constant is omitted, ξ_H was adjusted via temperature extrapolation. For an explanation of the categories, see Sect. 5. The number in parentheses denotes the statistical uncertainty in the last digit.
† Experimental VLE data are available for these binary systems

$$\mu_i{}^{\infty} = -k_{\mathrm{B}}T \ln \langle V \exp(-\psi_i/(k_{\mathrm{B}}T))\rangle / \langle V \rangle, \tag{4}$$

where V is the volume and the brackets represent the NpT ensemble average.

The residual chemical potential at infinite dilution $\mu_i{}^{\infty}$ and hence, the Henry's law constant H_i is directly related to the unlike solvent–solute interaction and indirectly to the like solvent–solvent interaction which yields the configurations of the solvent molecules. In these configurations, the solute test molecules are inserted. The mole fraction of the solute in the solvent is exactly zero, as required for infinite dilution, since the test molecules are ghost particles that are removed after the potential energy calculation and thus do not affect the solvent molecules. Simulations were performed in the liquid state at a specified temperature, and the pressure was set to the pure substance vapor pressure of the solvent, as described by the molecular model.

Based on pairwise additive molecular models, the Henry's law constant is determined by two different interactions: firstly, the like interaction between solvent molecules and, secondly, the unlike interaction between solvent and solute molecules. While the like interaction is fully defined by the solvent model, the unlike interaction requires some discussion: the unlike polar contribution is defined in a physically straightforward manner, simply using the laws of electrostatics. To define the unlike Lennard–Jones contribution between solute i and solvent S molecules, the modified Lorentz–Berthelot combining rule [100] was used

$$\sigma_{i\mathrm{S}} = \frac{\sigma_i + \sigma_{\mathrm{S}}}{2}, \tag{5}$$

and

$$\epsilon_{i\mathrm{S}} = \xi \cdot \sqrt{\epsilon_i \epsilon_{\mathrm{S}}}, \tag{6}$$

where ξ is the binary interaction parameter that mainly accounts for the unlike dispersion. The Henry's law constant is sensitive to ξ, i.e., it decreases with increasing ξ [18]. This is physically reasonable, as a higher solubility due to stronger unlike dispersive attraction is expected.

For the 29 binary mixtures which were studied in [6] and also in this work, values for ξ are available. These were obtained in [6] by an adjustment to a single experimental vapor pressure p at some finite mole fraction of the binary mixture. Such values are indicated by ξ_p in the following. On the basis of that binary interaction parameter ξ_p, the temperature dependence of the Henry's law constant was predicted here for the subgroup of 29 mixtures. As discussed below, in some cases significant deviations were encountered, in which case the binary interaction parameter was then readjusted to the experimental Henry's law constant data here, indicated by ξ_H. For the remaining 66 binary systems which were not studied in [6], ξ_H was adjusted in this work to H_i at some temperature, cf. Table 2.

In all simulations, 864 solvent molecules were used to evaluate the Henry's law constant. After an equilibration of 30,000 time steps, 200,000 production time steps of 1.5 fs were carried out inserting 3,456 test molecules into the liquid solvent after each time step. The Lennard–Jones long-range interactions beyond the cut-off radius were corrected, employing angle averaging as proposed by Lustig [101]. The dipolar interactions were corrected using the reaction field method [102]. The cut-off radius was at least 17.5 Å. The quadrupolar and also the mixed dipolar–quadrupolar interactions need no long-range corrections, as their contributions disappear by orientational averaging.

As discussed above, Widom's method has its limitations. Often, the solute molecules are smaller than the solvent molecules which is advantageous for the calculation of H_i. However, when the temperature is low and thus the saturated liquid solvent density is very high, the probability of successful test molecule insertions becomes very low. Then, the H_i calculation shows large statistical uncertainties or even a complete failure of that method. Nonetheless, molecular dynamics simulation in combination with Widom's method was used here, because it works at higher temperatures, and simulation data over a larger temperature range allow for a reasonable temperature extrapolation.

5 Results and Discussion

For 95 binary mixtures, the Henry's law constant H_i was determined as a function of temperature. The results are presented in the electronic supplementary material for each individual system in graphical form that contains the experimental data for comparison. There, it is distinguished graphically between the different experimental sources. The full numerical data set from simulation is provided in the electronic supplementary material as well, together with an estimate of the statistical uncertainty. Error bars were calculated by a block averaging method [103] and the error propagation law. Due to the fact that the error bars are predominantly within symbol size, they were omitted in the figures to achieve better visibility as the results for several binary

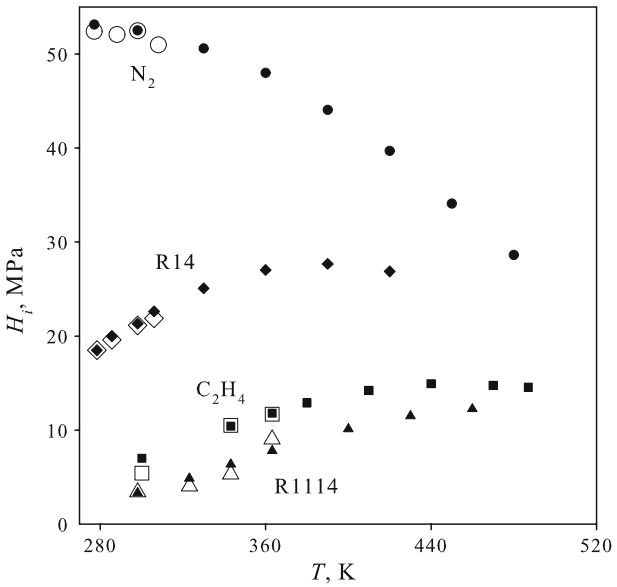

Fig. 1 Henry's law constant of N_2(●), C_2H_4(■), R14 (♦), and R1114 (▲) in liquid R113. Full symbols represent simulation results, empty symbols are experimental data [38,83,84,88]

mixtures are combined therein. In these figures, results for 37 of the 95 systems are shown as examples.

For this discussion, the 95 systems are grouped into six categories, cf. Table 2. The first category, containing 38 systems, is characterized by the presence of experimental data over a significant temperature range where a very good to excellent match with the simulation data was achieved. Eight such systems are shown in Figs. 1 and 2. The order of magnitude and also the temperature dependence of H_i vary. For example, H_i ranges from around 4 MPa for R1114 in R113, and increases with temperature (Fig. 1), to around 450 MPa for N_2 in CS_2 and decreases with temperature (Fig. 2). In the case of CH_4 in CS_2 (Fig. 2), H_i changes little with temperature in the range considered.

For the second category, containing the six systems Ne in R113, Ar in R10, N_2 in R114, R1132 in R113, R116 in R113, and Xe in R113, the experimental data are also available over a significant temperature range, but the simulation results show a qualitatively different temperature dependence. Three typical systems are shown in Fig. 3. Due to the fact that the binary interaction parameter was adjusted to experimental H_i data for five of the six systems, the data sets from simulation and experiment intersect. For the remaining system, Ar in R10, cf. Fig. 3, the binary interaction parameter was adjusted in [6] to experimental VLE data at 348.15 K. Around this temperature, the predicted H_i from simulation compares well with the experimental data, however, the temperature trend differs.

For the 44 mixtures in the first and second categories a comparably broad experimental database is available for the present assessment. As in 38 of the 44 cases, the temperature dependence of H_i from simulation agrees well with the experiment, it can be stated that molecular modeling and simulation generally yield good results.

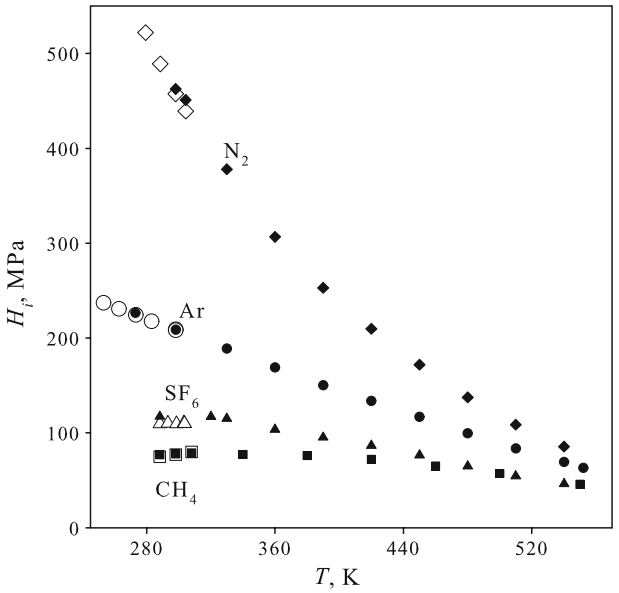

Fig. 2 Henry's law constant of Ar (●), CH_4(■), N_2(♦), and SF_6(▲) in liquid CS_2. Full symbols represent simulation results, empty symbols are experimental data [28,30,31]

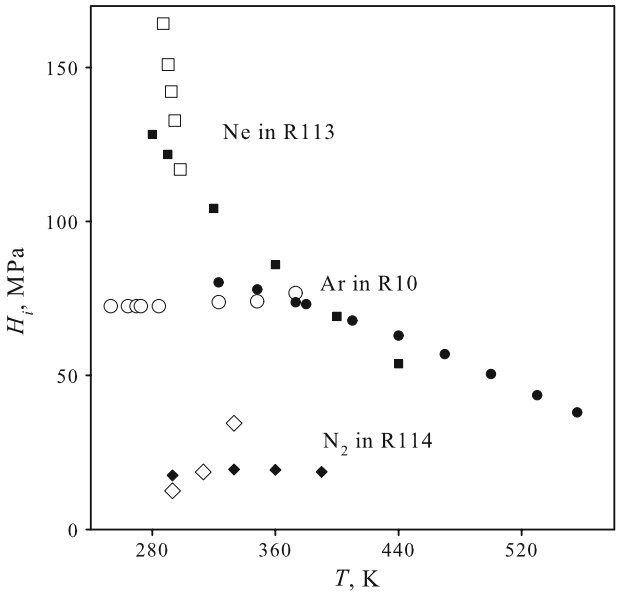

Fig. 3 Henry's law constant of Ar in liquid R10 (●), of Ne in liquid R113 (■) and of N_2 in liquid R114 (♦). Full symbols represent simulation results, empty symbols are experimental data [29,82,89]

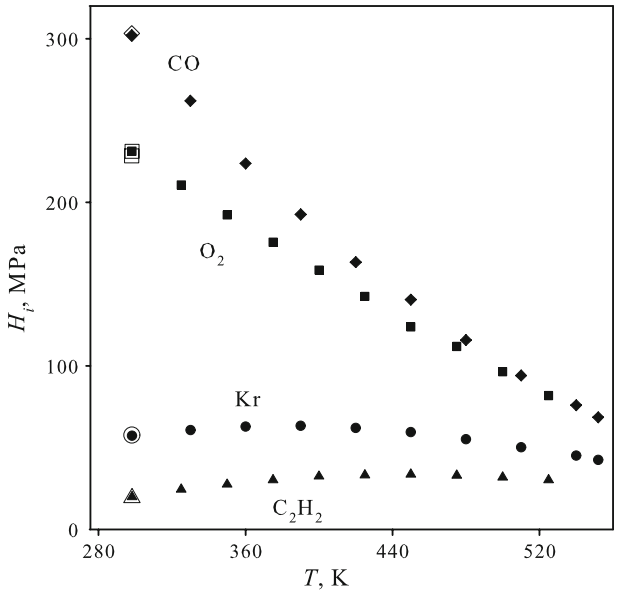

Fig. 4 Henry's law constant of Kr (●), O_2 (■), CO (♦), and C_2H_2 (▲) in liquid CS_2. Full symbols represent simulation results, empty symbols are experimental data [30,33,36]

The third category, containing 20 systems, is characterized by the presence of a single experimental H_i data point that is part of the temperature range where simulation was feasible. Due to the adjustment of ξ, the simulation data coincide with experiment; however, the presented temperature extrapolation cannot be assessed on the basis of experimental data. Figure 4 shows four typical systems.

For most mixtures, experimental H_i data are available only at low temperatures, typically below 360 K. Particularly for the studied polar solvents, the saturated liquid state is then highly dense, so that the calculation of the chemical potential of the solute at infinite dilution by Widom's test particle method fails for low temperatures. This also depends on the nature of the solute; the larger and more polar the solute molecule is, the higher is the minimum temperature where such a calculation is feasible.

In 16 cases, H_i could not be determined in the temperature range where experimental data are present, which is the fourth category. However, as can be seen in Figs. 5 and 6 for seven selected mixtures, both the experimental and simulation data allow for an overlapping extrapolation which can be regarded as satisfactory. Note that the binary interaction parameter for the three systems R12 in R10, Cl_2 in R140, and R1140 in R140 was adjusted in [6] to experimental VLE data at 297.75 K, 313 K, and 346.15 K, respectively, cf. Figs. 5 and 6. Thus, for these systems, it can be stated that the molecular mixture models yield correct and consistent H_i and VLE data. With respect to Widom's method, it can be seen in Fig. 6 that the H_i calculation at 330 K was feasible for R13 in R10, while for R14 in the same solvent, it was not.

Furthermore, the fifth category is also characterized by non-overlapping temperature ranges, but experimental data are present only for a single temperature or a

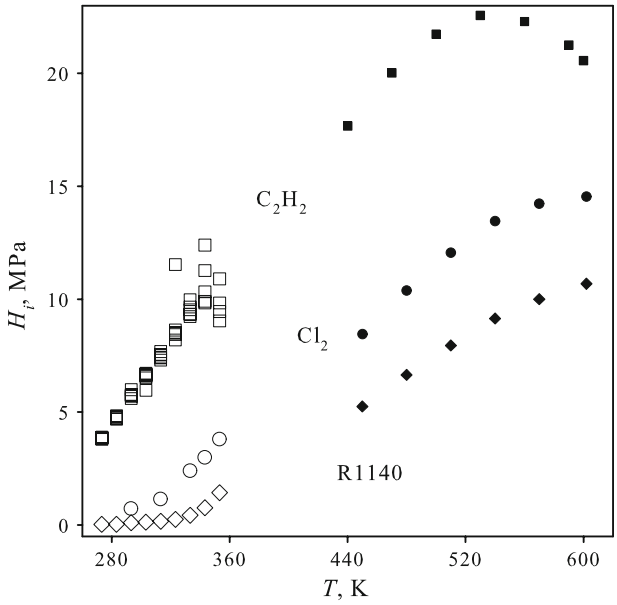

Fig. 5 Henry's law constant of Cl_2 (•), C_2H_2 (■), and R1140 (♦) in liquid R140. Full symbols represent simulation results, empty symbols are experimental data [90–92]

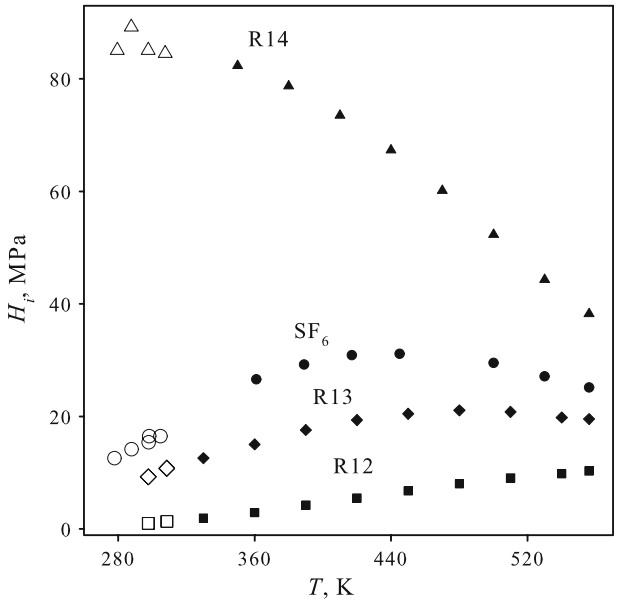

Fig. 6 Henry's law constant of SF_6 (•), R12 (■), R13 (♦), and R14 (▲) in liquid R10. Full symbols represent simulation results, empty symbols are experimental data [38,41,65]

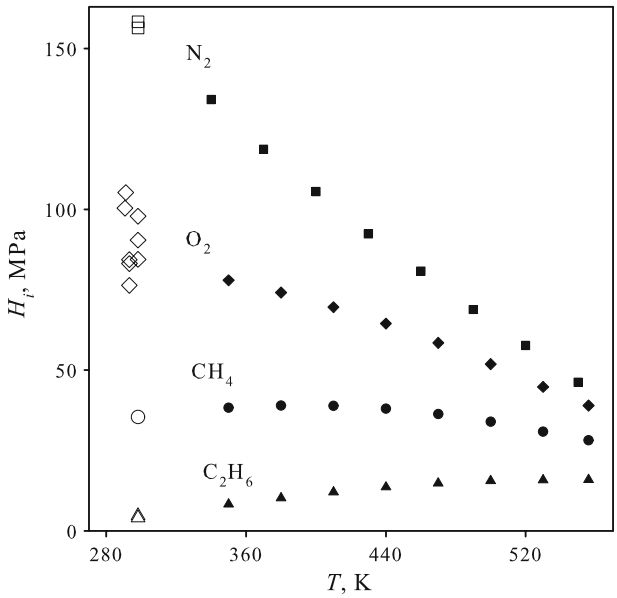

Fig. 7 Henry's law constant of CH_4(●), N_2(■), O_2(♦), and C_2H_6(▲) in liquid R10. Full symbols represent simulation results, empty symbols are experimental data [44,46,48,62]

very narrow temperature range. For the respective 12 systems, only the simulation data allow for an extrapolation which was found to be in satisfactory agreement with experiment. Four selected examples are shown in Fig. 7.

As indicated above, for 29 systems both experimental VLE and H_i data are available. For these systems, the binary interaction parameter has been adjusted to the vapor pressure at finite mole fractions in prior work [6], being indicated by ξ_p, leading to an excellent match between experiment and simulation with respect to the VLE data. For a subgroup of 20 systems, it was found here that these molecular mixture models are capable of yielding correct and consistent H_i and VLE data. Four such systems are shown in Fig. 8 as examples.

For the remaining nine systems, the predicted H_i data deviate from the experiment so that the binary interaction parameter was readjusted in these cases, labeled by ξ_H. This issue is illustrated in Figs. 9 and 10 for six systems. For example, in the case of CO_2 in CS_2, cf. Fig. 9, the H_i values predicted on the basis of ξ_p are too low by around 30 %, but the temperature trend is satisfactory. Decreasing the binary interaction parameter by approximately 0.04 shifts H_i onto to the experimental data. For other systems, e.g., Ar in R113, cf. Fig. 10, the H_i values predicted on the basis of ξ_p are too high, so that $\xi_H < \xi_p$. It was observed that the influence of the binary interaction parameter on H_i is weaker for higher temperatures.

Figure 11 lists the 29 systems where both experimental VLE and H_i data are available, comparing their optimal binary interaction parameters ξ_p from [6] and ξ_H from this work. As can be seen, only in a few cases, e.g., C_2H_2 in R10 or R23 in R114, they strongly differ.

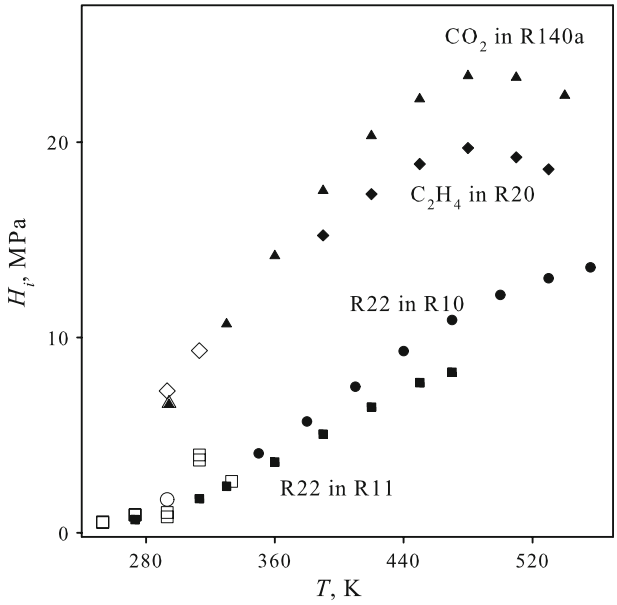

Fig. 8 Henry's law constant of R22 in liquid R10 (●), R22 in liquid R11 (■), C_2H_4 in liquid R20 (♦), and CO_2 in liquid R140a (▲). Full symbols represent simulation results where the binary parameter ξ_p was adjusted to the vapor pressure in [6], empty symbols are experimental data [59,63,66,75]

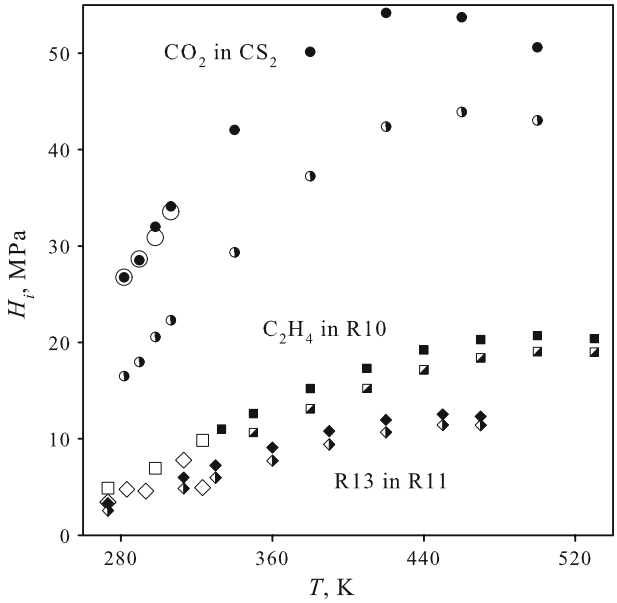

Fig. 9 Henry's law constant for different binary systems. Full symbols represent simulation results where the binary parameter ξ_H was adjusted to the Henry's law constant in this work, semi-filled symbols represent simulation results where the binary parameter ξ_p was adjusted to the vapor pressure in [6], empty symbols are experimental data: CO_2 in liquid CS_2(●), $\xi_H = 0.877$, $\xi_p = 0.918$, [28,31,57]; C_2H_4 in liquid R10 (■), $\xi_H = 0.978$, $\xi_p = 1.003$, [61,63]; R13 in liquid R11 (♦), $\xi_H = 0.953$, $\xi_p = 0.975$, [75]

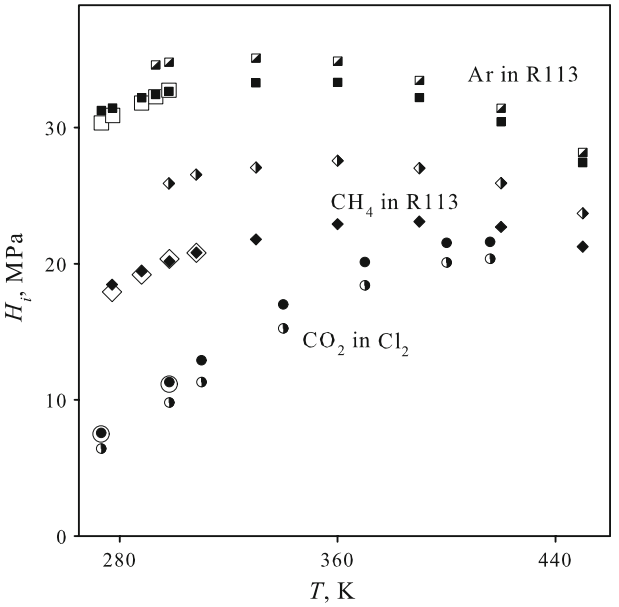

Fig. 10 Henry's law constant for different binary systems. Full symbols represent simulation results where the binary parameter ξ_H was adjusted to the Henry's law constant in this work, semi-filled symbols represent simulation results where the binary parameter ξ_p was adjusted to the vapor pressure in [6], empty symbols are experimental data: CO_2 in liquid Cl_2 (●), $\xi_H = 0.920$, $\xi_p = 0.936$, [25]; Ar in liquid R113 (■), $\xi_H = 1.027$, $\xi_p = 1.012$, [83]; CH_4 in liquid R113 (♦), $\xi_H = 1.044$, $\xi_p = 0.997$, [83]

Finally, for the three mixtures Ne in R10, CO in R140a, and CO_2 in R150B2, constituting the sixth category, the present modeling approach did not yield reasonable results. The simulation data according to the Berthelot rule, i.e., $\xi = 1$, were found to be very far off the experimental data which would require altering ξ by an unphysically large extent, e.g, $\xi > 2$ in the case of CO in R140a. It should be noted that the 1CLJ model for Ne performs poorly with respect to VLE data [6]. This is confirmed, as for both mixtures containing Ne studied here, i.e., Ne in R10 and Ne in R113 (wrong temperature dependence), unsatisfactory results were achieved.

Another aspect that can be studied on the basis of the present simulation data is the general temperature trend of the Henry's law constant for different solutes in a given solvent. For example, for the solvent R10, a total of 19 solutes was investigated. These simulation results are combined in Fig. 12, showing that the H_i values at low temperatures cover a band of around 130 MPa. With increasing temperature, the data sets for the different solutes converge, covering a band of around 35 MPa at the critical temperature of the solvent. For the solvent CS_2, where 15 solutes were investigated here, a similar behavior was found. Thus, it can be concluded that the Henry's law constant at high temperatures is less influenced by the solute properties through the unlike interaction, but mainly by the like solvent–solvent interaction.

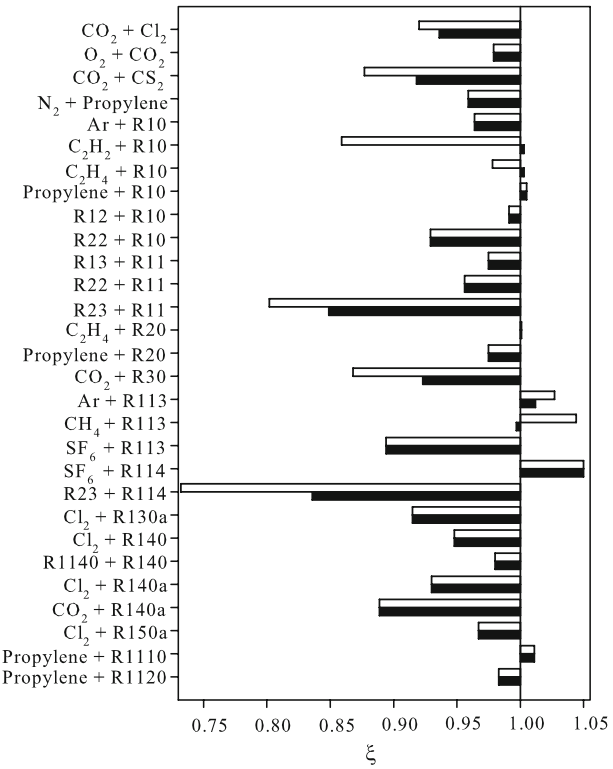

Fig. 11 Comparison of the binary interaction parameter ξ_H that was adjusted to the Henry's law constant in this work (*full bars*) to the binary interaction parameter ξ_p that was adjusted to the vapor pressure in [6] (*empty bars*)

6 Conclusion

It was shown that molecular simulation is a reliable method for investigating the Henry's law constant of gases dissolved in liquid solvents. To verify this issue, an extensive simulation effort was made to cover 95 binary mixtures in a combinatorial way. The molecular models employed in many cases oversimplify the molecular features of the substance that they represent. However, it was found that the molecular models are usually able to compensate such oversimplifications and adequately cover the gas solubility effects.

To optimally represent the phase behavior of all of the binary mixtures studied, the unlike dispersive energy parameter was adjusted to a single experimental Henry's law constant or the binary vapor pressure of each mixture. It was found that the Berthelot rule is a good choice. In 50 % of the cases studied, unlike dispersion was modified by 5 % or less. On average, unlike dispersion should be slightly weaker than the Berthelot rule suggests.

Based on these mixture models, the temperature dependence of the Henry's law constant was predicted and compared to the available experimental data. For the large

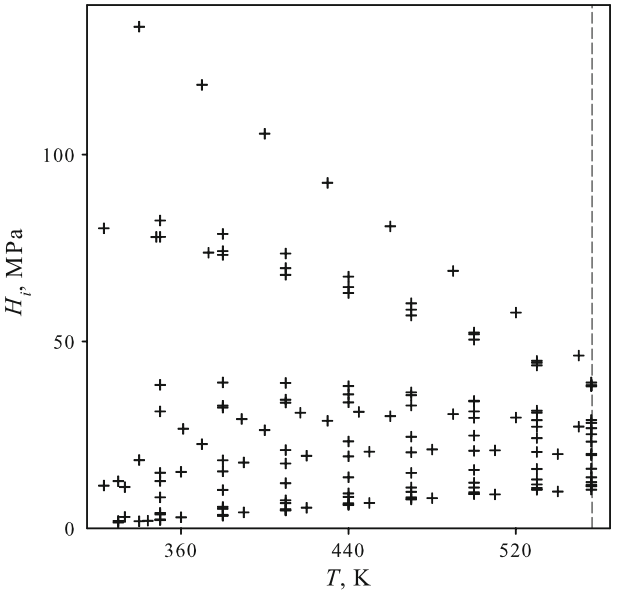

Fig. 12 Henry's law constant of the 19 solutes Ar, Kr, CH_4, N_2, O_2, Cl_2, CO_2, C_2H_2, C_2H_4, C_2H_6, Propylene, SF_6, R12, R13, R14, R22, R23, R40, and R161 in liquid R10 from simulation (+). The *dashed line* indicates the critical temperature of the solvent

majority of systems that can be assessed in this sense, a good agreement was found. Furthermore, it was shown that the models are generally capable of yielding correct and consistent phase equilibrium data at infinite dilution and also at finite mole fractions.

For high temperatures, it was found for a given solvent that the Henry's law constant of different solutes converges to a narrow band. This indicates that this thermophysical property is then mainly determined by the solvent–solvent interaction.

Due to their numerical efficiency and accuracy, those molecular mixture models that were found to yield consistent data are also well suited to be used in simulations on a larger scale to investigate processes such as absorption, adsorption, evaporation, flow, etc.

Acknowledgments We gratefully acknowledge Deutsche Forschungsgemeinschaft for funding this project. The presented research was conducted under the auspices of the Boltzmann-Zuse Society of Computational Molecular Engineering (BZS), and the simulations were performed on the national super computer NEC SX-8 at the High Performance Computing Center Stuttgart (HLRS) and on the HP X6000 super computer at the Steinbuch Centre for Computing, Karlsruhe. We would like to thank Xijun Fu and Qingyun Li for handling numerous simulation runs and helping to prepare the material for publication.

References

1. T.M. Letcher (ed.), *Developments and Applications in Solubility* (The Royal Society of Chemistry, Cambridge, 2007)
2. J.M. Smith, H.C. Van Ness, M.M. Abbott, *Introduction to Chemical Engineering Thermodynamics*, 5th edn. (McGraw-Hill, New York, 1996)

3. I.R. Krichevsky, J.S. Kasarnovsky, J. Am. Chem. Soc. **57**, 2168 (1935)
4. J. Vrabec, J. Stoll, H. Hasse, J. Phys. Chem. B **105**, 12126 (2001)
5. J. Stoll, J. Vrabec, H. Hasse, J. Chem. Phys. **119**, 11396 (2003)
6. J. Vrabec, Y.-L. Huang, H. Hasse, Fluid Phase Equilib. **279**, 120 (2009)
7. K.S. Shing, K.E. Gubbins, K. Lucas, Mol. Phys. **65**, 1235 (1988)
8. J. Stecki, A. Samborski, S. Toxvaerd, Mol. Phys. **70**, 985 (1990)
9. R.J. Sadus, J. Phys. Chem. B **101**, 3834 (1997)
10. S. Murad, S. Gupta, Chem. Phys. Lett. **319**, 60 (2000)
11. A. Lotfi, J. Fischer, Mol. Phys. **66**, 199 (1989)
12. G.C. Boulougouris, J.R. Errington, I.G. Economou, A.Z. Panagiotopoulos, D.N. Theodorou, J. Chem. Phys. B **104**, 4958 (2000)
13. G.C. Boulougouris, E.C. Voutsas, I.G. Economou, D.N. Theodorou, D.P. Tassios, J. Chem. Phys. B **105**, 7792 (2001)
14. I.G. Economou, Fluid Phase Equilib. **183–184**, 259 (2001)
15. M. Lísal, W.R. Smith, K. Aim, Fluid Phase Equilib. **228–229**, 345 (2005)
16. S. Murad, S. Gupta, Fluid Phase Equilib. **187–188**, 29 (2001)
17. F. Case, A. Chaka, D.G. Friend, D. Frurip, J. Golab, P. Gordon, R. Johnson, P. Kolar, J. Moore, R.D. Mountain, J. Olson, R. Ross, M. Schiller, Fluid Phase Equilib. **236**, 1 (2005)
18. T. Schnabel, J. Vrabec, H. Hasse, Fluid Phase Equilib. **233**, 134 (2005) and **239**, 125 (2006)
19. Y. Boutard, Ph. Ungerer, J.M. Teuler, M.G. Ahunbay, S.F. Sabater, J. Pérez-Pellitero, A.D. Mackie, E. Bourasseau, Fluid Phase Equilib. **236**, 25 (2005)
20. E.C. Cichowski, T.R. Schmidt, J.R. Errington, Fluid Phase Equilib. **236**, 58 (2005)
21. C. Wu, X. Li, J. Dai, H. Sun, Fluid Phase Equilib. **236**, 66 (2005)
22. L. Zhang, J.I. Siepmann, Theor. Chem. Acc. **115**, 391 (2006)
23. B. Widom, J. Chem. Phys. **39**, 2808 (1963)
24. J. Gmehling, J. Rarey, J. Menke, *Dortmunder Datenbank* (Mixture Properties, Version 1.3.0.211, 2004)
25. W.F. Krieve, D.M. Mason, J. Phys. Chem. **60**, 374 (1956)
26. R.D. Ackley, K.J. Notz, *Distribution of Xenon between Gaseous and Liquid* CO_2 (Technical Report ORNL-5122, Oak Ridge National Lab. TN, USA, 1976)
27. A. Fredenslund, J. Mollerup, O. Persson, J. Chem. Eng. Data **17**, 440 (1972)
28. J.C. Gjaldbaek, H. Niemann, Acta Chem. Scand. **12**, 611 (1958)
29. L.W. Reeves, J.H. Hildebrand, J. Am. Chem. Soc. **79**, 1313 (1957)
30. R.J. Powell, J. Chem. Eng. Data **17**, 302 (1972)
31. Y. Kobatake, J.H. Hildebrand, J. Phys. Chem. **65**, 331 (1961)
32. J.C. Gjaldbaek, J.H. Hildebrand, J. Am. Chem. Soc. **71**, 3147 (1949)
33. J.C. Gjaldbaek, Acta Chem. Scand. **6**, 623 (1952)
34. A.D. Raskina, V.I. Zetkin, E.V. Zakharov, I.M. Kolesnikov, V.I. Kosorotov, J. Appl. Chem. (USSR) **45**, 1374 (1972)
35. J.C. Gjaldbaek, Acta Chem. Scand. **7**, 537 (1953)
36. Y. Miyano, W. Hayduk, Can. J. Chem. Eng. **59**, 746 (1981)
37. A. Sahgal, H.M. La, W. Hayduk, J. Chem. Eng. **56**, 354 (1978)
38. G. Archer, J.H. Hildebrand, J. Phys. Chem. **67**, 1830 (1963)
39. Yu.P. Blagoi, N.A. Orobinskii, Russ. J. Phys. Chem. **39**, 1073 (1965)
40. H.C. Miller, L.S. Verdelli, J.F. Gall, Ind. Eng. Chem. **43**, 1126 (1951)
41. T. Tominaga, R. Battino, H.K. Gorowara, R.D. Dixon, E. Wilhelm, J. Chem. Eng. Data **31**, 175 (1986)
42. E.B. Graham, K.E. Weale, Prog. Int. Res. Therm. Trans. Prop. 153 (1962)
43. F. Körösy, Trans. Faraday Soc. **33**, 416 (1937)
44. A. Lannung, J.C. Gjaldbaek, Acta Chem. Scand. **14**, 1124 (1960)
45. T. Akimoto, T. Nitta, T. Katayama, J. Chem. Eng. (Japan) **17**, 637 (1984)
46. V.M. Gorbachev, T.V. Tretyakov, Zavod. Lab. (USSR) **32**, 796 (1966)
47. J.K. Wolfe, Refrig. Eng. **59**, 704 (1951)
48. P. Luehring, A. Schumpe, J. Chem. Eng. Data **34**, 250 (1989)
49. N.K. Naumenko, *Investigation on the Solubility of Oxygen in Organic Solvents*, Thesis (1970), p. 3
50. P. Schlaepfer, T. Audykowski, A. Bukowiecki, Schweizer Archiv für Wiss. u. Technik **15**, 299 (1949)
51. E. Sinn, K. Matthes, E. Naumann, Z. Wiss, Friedrich-Schiller-Univ. Jena, Math.-Naturwiss. R. **16**, 523 (1967)

52. V.T. Vdovichenko, V.I. Kondratenko, Khim. Prom. (USSR) **43**, 290 (1967)
53. L.M. Kogan, N.S. Koltsov, N.D. Litvinov, Russ. J. Phys. Chem. **37**, 1040 (1963)
54. T.L. Smith, J. Phys. Chem. **59**, 188 (1955)
55. C.M. Blair, D.M. Yost, J. Am. Chem. Soc. **55**, 4489 (1933)
56. N.W. Taylor, J.H. Hildebrand, J. Am. Chem. Soc. **45**, 682 (1923)
57. G. Just, Z. Phys. Chem. **37**, 342 (1901)
58. M. Takahashi, Y. Kobayashi, H. Takeuchi, J. Chem. Eng. Data **27**, 328 (1982)
59. H. Hsu, D. Campbell, Aerosol Age **9**, 34 (1964)
60. H. Takeuchi, M. Fujine, T. Sato, K. Onda, J. Chem. Eng. (Japan) **8**, 252 (1975)
61. N. Brueckl, J.I. Kim, Z. Phys. Chem., Neue Folge **126**, 133 (1981)
62. R. Jadot, J. Chim. Phys. Phys.-Chim. Biol. **6**, 1036 (1972)
63. B.I. Konobeev, V.V. Lyapin, Khim. Prom. (USSR) **43**, 114 (1967)
64. W. Hayduk, S.C. Cheng, Can. J. Chem. Eng. **48**, 93 (1970)
65. E. Wilhelm, R. Battino, J. Chem. Thermodyn. **3**, 379 (1971)
66. R.G. Makitra, Ya.N. Pirig, T.I. Politanskaya, F.B. Moin, Russ. J. Phys. Chem. **55**, 424 (1981)
67. Anonymous, *Löslichkeit von F*23 *und HCl in verschiedenen Lösungsmitteln* (Confident. Comp. Res. Rep., Rep. No. LC4912, 1970; cf. [24])
68. Anonymous, *Löslichkeit von HCl und F*23 *in verschiedenen Lösungsmitteln*, (Confident. Comp. Res. Rep., Rep. No. LC4914, 1970; cf. [24])
69. P. Sies, J. Krafczyk, Unpublished Data (1992); cf. [24]
70. J. Krafczyk, Unpublished Data (1991); cf. [24]
71. Yu.G. Mamedaliev, S. Musakhanly, Zh. Prikl. Khim. (USSR) **13**, 735 (1940)
72. J. Horiuti, Sci. Pap. Inst. Phys. Chem. Res. (Japan) **17**, 125 (1931)
73. R.G. Makitra, T.I. Politanskaya, F.B. Moin, Y.N. Pirig, T.S. Politanskaya, J. Appl. Chem. (USSR) **56**, 2048 (1984)
74. R.G. Makitra, F.B. Moin, T.I. Politanskaya, J. Phys. Chem. (USSR) **53**, 572 (1979)
75. M. Kriebel, H.J. Loeffler, Kältetechnik **18**, 34 (1966)
76. Anonymous, *Löslichkeit von gasförmigem F*13, *F*22 *und F*23 *in flüssigem F*11 (Confident. Comp. Res. Rep., Rep. No. LC4994, 1969; cf. [24])
77. T. Nitta, Y. Nakamura, H. Ariyasu, T. Katayama, J. Chem. Eng. (Japan) **13**, 97 (1980)
78. F. Fischer, G. Pfleiderer, Z. Anorg. Chem. **124**, 61 (1922)
79. N.F. Giles, L.C. Wilson, G.M. Wilson, W.V. Wilding, J. Chem. Eng. Data **42**, 1067 (1997)
80. F.H. Vonderheiden, J.W. Eldridge, J. Chem. Eng. Data **8**, 20 (1963)
81. K.E. Doering, FIZ Report, 1201 (1965)
82. R.G. Linford, J.H. Hildebrand, Trans. Faraday Soc. **66**, 577 (1970)
83. H. Hiraoka, J.H. Hildebrand, J. Phys. Chem. **68**, 213 (1964)
84. Y.P. Sokolov, A.I. Konshin, J. Appl. Chem. (USSR) **62**, 1310 (1989)
85. D.A. Armitage, R.G. Linford, D.G.T. Thornhill, Ind. Eng. Chem. Fundam. **17**, 362 (1978)
86. R.G. Linford, J.H. Hildebrand, J. Phys. Chem. **73**, 4410 (1969)
87. H. Jaster, P.G. Kosky, J. Chem. Eng. Data **21**, 66 (1976)
88. Yu.A. Sokolov, A.I. Konshin, S.V. Sokolov, J. Appl. Chem. (USSR) **60**, 2523 (1988)
89. V.D. Williams, J. Chem. Eng. Data **4**, 92 (1959)
90. O.V. Efstigneev, M.B. Santimova, S.G. Dunaev, S.B. Levanova, Khim. Prom. (USSR) **6**, 342 (1985)
91. R.G. Makitra, F.B. Moin, Ya.N. Pirig, T.I. Politanskaya, J. Appl. Chem. (USSR) **60**, 663 (1987)
92. R.G. Makitra, F.B. Moin, Ya.N. Pirig, T.I. Politanskaya, J. Appl. Chem. (USSR) **62**, 2567 (1990)
93. S.M. Danov, Yu.D. Golubev, Khim. Prom. (USSR) **44**, 116 (1968)
94. J.C. Gjaldbaek, E.K. Anderson, Acta Chem. Scand. **8**, 1398 (1954)
95. E. Otsuka, M. Takada, Nenryo-Kyokai-Shi **42**, 229 (1963)
96. O.Y. Guzechak, V.N. Sarancha, I.M. Romanyuk, O.M. Yavorskaya, G.P. Churik, J. Appl. Chem. (USSR) **57**, 1662 (1985)
97. U.K. Deiters, Fluid Phase Equilib. **132**, 265 (1997)
98. J. Stoll, J. Vrabec, H. Hasse, J. Fischer, Fluid Phase Equilib. **179**, 339 (2001)
99. J. Stoll, J. Vrabec, H. Hasse, Fluid Phase Equilib. **209**, 29 (2003)
100. T. Schnabel, J. Vrabec, H. Hasse, J. Mol. Liq. **135**, 170 (2007)
101. R. Lustig, Mol. Phys. **65**, 175 (1988)
102. M.P. Allen, D.J. Tildesley, *Computer Simulation of Liquids* (Clarendon Press, Oxford, 1987)
103. H. Flyvbjerg, H.G. Petersen, J. Chem. Phys. **91**, 461 (1989)